Design of a Coupled Feed Structure With Cavity Walls for Extremely Small Anti-Jamming Arrays

GANGIL BYUN [ID][1], (Member, IEEE), **JUN HUR**[2], (Student Member, IEEE), **SEUNG-SEOK KANG**[3],
SEOK BO SON[3], **AND HOSUNG CHOO** [ID][2], (Member, IEEE)

[1]School of Electrical and Computer Engineering, Ulsan National Institute of Science and Technology, Ulsan 44919, South Korea
[2]School of Electronic and Electrical Engineering, Hongik University, Seoul 04066, South Korea
[3]Navcours Co., Ltd., Deajeon 34014, South Korea

Corresponding author: Hosung Choo (hschoo@hongik.ac.kr)

ABSTRACT This paper proposes a coupled-feed structure accompanied by cavity walls for an extremely small four-element array with an aperture size of less than 0.4λ. The feeding loop of the proposed structure is connected to two output ports of a hybrid chip coupler, and the radiating loop is coupled to the feeding loop through near electromagnetic fields confined within the substrates. This structure allows to increasing the effective dielectric constant of the antenna, which helps to miniaturize the aperture size of the antenna. Another advantage of the proposed structure is that the effective dielectric constant can be adjusted by varying the height of the cavity walls. To verify the operating principles, an equivalent circuit is built, and variations of magnetic field distributions are also observed. Furthermore, performances on interference mitigation are evaluated based on the power inversion algorithm. The results confirm that the proposed structure is suitable to replace current single-antenna systems for an additional capability of effective interference mitigation in such a restricted area.

INDEX TERMS Small antenna array, microstrip antenna, coupled feed, anti-jamming, controlled reception pattern antenna.

I. INTRODUCTION

In recent satellite navigation systems, there has been a growing demand to replace a single microstrip antenna with an antenna array, especially for aeronautic vehicles [1]. The greatest advantage of this replacement is that the system becomes capable of steering pattern nulls toward directions of interferences, such as intentional jammers [2]–[6]. This approach is also known as a controlled reception pattern antenna (CRPA) operation, and the nulling direction is adjusted by varying phase excitations at antenna ports to keep the jamming power as low as the noise floor [7]. However, in most of the cases, the space occupied by the single antenna is limited to a few centimeters, which is less than a half wavelength in the GPS L bands. Thus, there has been a lot of effort to miniaturize the array aperture to fit multiple antennas in the given space without structural modification. General approaches to the aperture miniaturization are the use of high-dielectric ceramic substrates [8], [9], slot

insertion [10], [11], and shorting pins [12], [13]. However, the antenna with a higher dielectric constant has a lower aperture efficiency with increased sensitivity of fabrication error [14]. In addition, the insertion of slots and shorting pins to microstrip patches often exhibits a narrow bandwidth for both the impedance matching and the axial ratio [15]. Note that the narrow bandwidth is not preferred in small arrays because antenna characteristics are easily degraded by the effect of strong mutual coupling causing unexpected frequency shifts [16].

In this paper, we propose a coupled-feed structure combined with cavity walls to enhance the effective dielectric constant for an extremely small four-element CRPA array. The proposed structure consists of a lower feeding loop and an upper radiating loop, and these loops are printed on the top of thick ceramic substrates. The feeding loop is connected to two output ports of an external hybrid chip coupler for circular polarization, and the radiating loop is electromagnetically coupled to the feeding loop. This structure is originally proposed in [17] by the same author to achieve the frequency-insensitive behavior between dual

The associate editor coordinating the review of this manuscript and approving it for publication was Raghvendra Kumar Kumar Chaudhary.

resonances in the GPS L1 and L2 bands; however, in this paper, we present a different perspective with a modified structure for a single resonance. The major contribution of our work is that we add cavity walls on lateral faces of the substrates to increase the effective dielectric constant for further miniaturization. Note that the antenna size without the cavity in [17] cannot be further reduced unless a higher dielectric constant is employed. In addition, the conventional role of the cavity structure is to realize the Fabry-Perot effect for increased directivity [18], which is distinguished from our approach. As a result, the aperture size of 0.113λ is achieved for each individual antenna, and the total array aperture including its ground is reduced to 0.4λ at 1.575 GHz. To verify the feasibility, the four-element array is fabricated, and its antenna characteristics are measured in a full anechoic chamber. Operating principles are interpreted by modeling an equivalent circuit, and variations of magnetic field distributions are also observed to analyze how the use of cavity walls increases the effective dielectric constant. In addition, the null steering performances are further demonstrated by applying the power inversion algorithm according to different jamming powers [19]. The results confirm that the proposed structure is suitable to miniaturize its aperture size for extremely small arrays and allows the capability of effective interference mitigation in such a restricted area.

II. PROPOSED ANTENNA ARRAY

A. DESIGN APPROACH

Fig. 1 shows a geometry of the proposed four-element array that is mounted on a printed circuit board (PCB) with a maximum aperture diameter of 76.3 mm (0.4λ at 1.575 GHz) and thickness h_g. The PCB embeds circuits of external hybrid chip couplers at the bottom, and its shape mimics the given space that is originally assigned for a stand-alone GPS antenna. To place four elements within the given space, the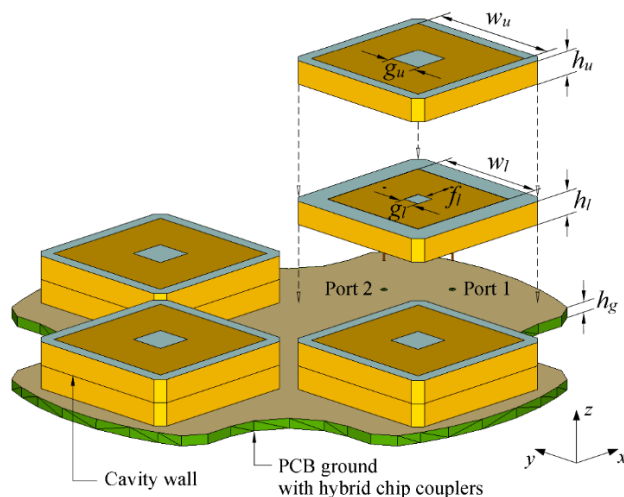 maximum aperture size of each array element should be restricted to 21.5×21.5 mm^2, which is $0.113\lambda \times 0.113\lambda$ at 1.575 GHz. Although the use of high permittivity is a well-known approach to miniaturize microstrip patch antennas, it causes the reduction of radiation efficiency, which is not desired in such long-distance satellite signal reception. Thus, instead of further increasing the permittivity, we employ the cavity wall onto the lateral faces of ceramic substrates to maximize the effective dielectric constant. The use of cavity walls increases the effective dielectric constant by confining fields inside the cavity wall, which allows fringing fields to remain within the substrates. Then, the electromagnetically coupled feed structure, presented in [17], is adopted because of two advantages [20]–[23]. First, the edge length is reduced to about $\lambda/4$, which is half of a conventional square patch antenna ($\cong \lambda/2$), since the circumference of the square loop is designed to be about one wavelength (λ). Second, when the two loops are vertically well-aligned, the magnetic flux generated by the feeding loop helps to increase the strength of magnetic coupling between the loops. In our approach, ceramic substrates with dielectric properties of $\varepsilon_r = 20$ and $\tan\delta = 0.002$ are used, and their thicknesses are indicated by h_l and h_u. The feeding loop is connected to the external chip coupler through two via pins with a phase difference of 90°, and the feeding positions are determined by f_l. The microstrip loops have outer edge lengths of w_l and w_u with inner edge lengths of g_l and g_u, and they are adjusted to vary the ratio between electric and magnetic coupling strengths for better impedance matching properties. The four corners of the substrates are truncated by 1.1 mm so that the cavity walls of nearby antennas are electrically separated without a physical contact for lower mutual coupling. Note that the circumference of the feeding loop is determined to be one wavelength at a higher frequency band (> 2 GHz), while the radiating loop resonates at 1.575 GHz. This is a distinguished approach compared to [17] whose target resonant frequencies are 1.227 GHz and 1.575 GHz using lower and upper loops, respectively. As a result, the effective dielectric constant, denoted by ε_{eff}, is increased from 18 to 19.5, and the target aperture size of 21.5×21.5 mm^2 ($0.113\lambda \times 0.113\lambda$) is achieved.

B. FABRICATION AND MEASUREMENT

The proposed structure is tuned to maximize the bore-sight gain of active element patterns at 1.575 GHz [24], and the optimized values are listed in Table 1. As we aimed, the feeding and radiating loops have circumferences of 31.6 mm and 45.6 mm, which are about one wavelength at 2.25 GHz and 1.575 GHz, respectively. Fig. 2 shows a fabricated array with the PCB ground embedding antenna feeding networks at the bottom. Each feeding network is designed to excite the feeding loop with a phase difference of 90° for circular polarization and consists of hybrid chip couplers (model: XC1400P-03S, Anaren Inc., Syracuse, NY, USA), 50-Ω termination chips, and coplanar waveguides.

Fig. 3(a) presents a comparison of measured and simulated reflection coefficients that are calculated at Ant. 1 while
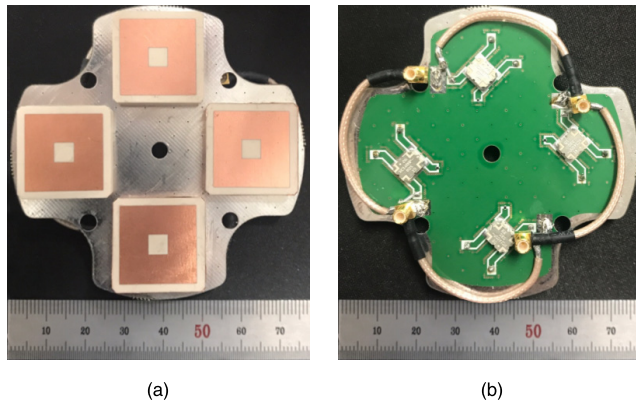

FIGURE 1. Geometry of the proposed four-element array.

FIGURE 2. Photograph of the fabricated array. (a) Top view. (b) Bottom view.

TABLE 1. Design parameters of the proposed array.

| Parameter	Value	Description
w_u	18.2 mm	Edge length of radiating loop
w_l	15.4 mm	Edge length of feeding loop
g_u	4.6	Gap width of radiating loop
g_l	0.4 mm	Gap width of feeding loop
h_u	3 mm	Substrate thickness of radiating loop
h_l	3 mm	Substrate thickness of feeding loop
h_g	1.3 mm	Substrate thickness of PCB ground
f_l	5.6 mm	Feeding distance in feeding loop

other ports are terminated by 50-Ω loads. In our simulation, scattering parameters of the two pins, denoted as S_{11}, S_{12}, S_{21}, and S_{22}, are obtained from full-wave electromagnetic simulations [25]. Then, these parameters are used to calculate the reflection coefficient with an assumption that the hybrid coupler has an ideal response, as given by

$$\Gamma = -\frac{1}{2} \{(-S_{11} + S_{22}) + j(S_{12} + S_{21})\}. \qquad (1)$$

Due to the use of hybrid chip couplers, the antenna shows broadband characteristics, and both results show a good agreement with simulated and measured values of -13.6 dB and -12.5 dB at 1.575 GHz. Fig. 3(b) provides mutual coupling, denoted by $|S_{21}|$ and $|S_{31}|$, as a function of frequency. The measured $|S_{21}|$ is -9.7 dB, and the simulated $|S_{21}|$ is -9.9 dB for an inter-element spacing of 31.1 mm (0.16λ). These values are consistently greater than $|S_{31}|$ whose measured and simulated values are -20.7 dB and -19.3 dB, respectively, which is due to the larger separation of 44 mm (0.23λ).

Fig. 4 shows simulated bore-sight gains of active element patterns in comparison with measured results. The blue line indicates simulated data, and the measured data are specified by a red line and '*' markers, which are obtained in semi- and full-anechoic chambers. We present the results obtained zin the semi-anechoic chamber as well to present a continuous curve, because the maximum number of frequency points
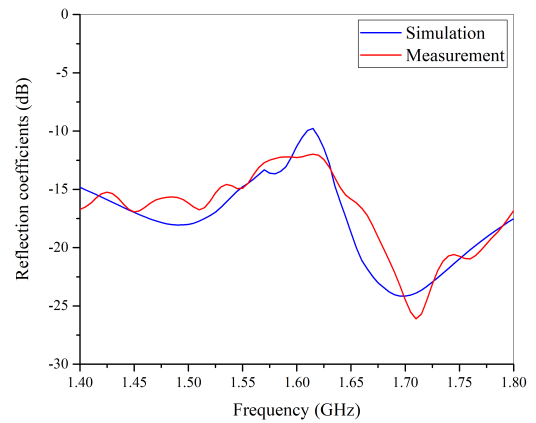
(a)
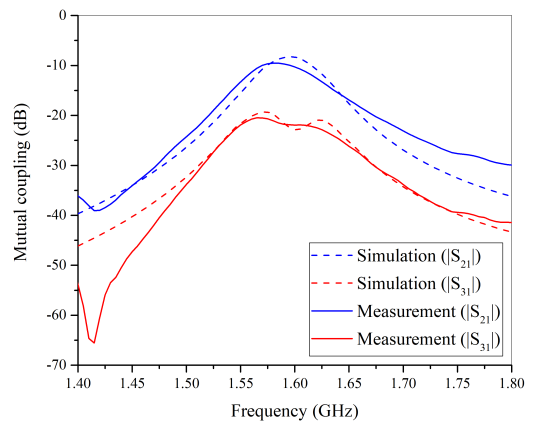
(b)

FIGURE 3. Measured and simulated scattering parameters. (a) Reflection coefficients. (b) Mutual coupling.
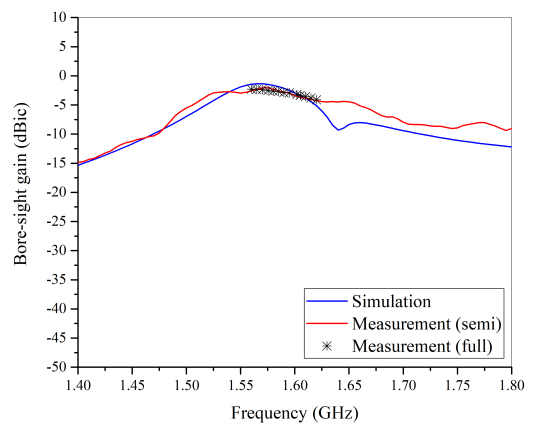

FIGURE 4. Measured and simulated bore-sight gains of Ant. 1.

that the full-anechoic chamber provides is limited to twenty. Measured values at 1.575 GHz are -2.51 dBic (full) and -2.05 dBic (semi) and are in the same order of magnitude with a simulated value of -1.46 dBic. Note that the bore-sight
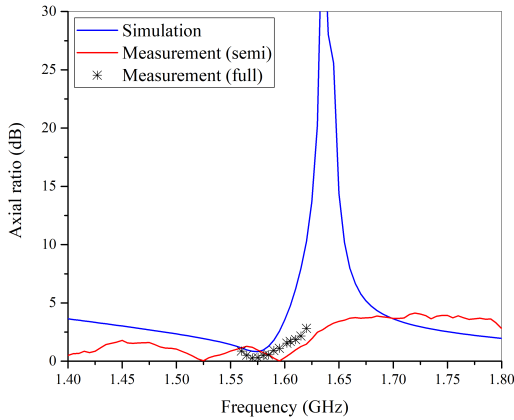
FIGURE 5. Measured and simulated axial ratios of Ant. 1.

gain without the mutual coupling effect is 2.42 dBic with the radiation efficiency of 58.9%; however, the mutual coupling degrades the radiation efficiency to 27.5%, which results in the gain reduction of about 3.9 dB. Fig. 5 shows measured and simulated axial ratios in the bore-sight direction. Both results confirm that the antenna is circularly polarized with measured results of 0.31 dB (full) and 0.96 dB (semi), which are similar to the simulated value of 0.82 dB.

Figs. 6(a) and 6(b) provide active element patterns in *zx*- and *yz*-planes of Ant. 1 at 1.575 GHz. Solid lines show patterns with the right-hand circular polarization, and dashed lines present those of the cross polarization. In *zx*-plane, the maximum measured gain is −2.24 dBic at $\theta = -10°$ with the measured cross-polarization level of −22.5 dB in the bore-sight direction. Similarly in the *yz*-plane, the maximum gain of −1.92 dB is slightly steered toward $\theta = 10°$, and the cross-polarization level is measured and simulated as −20.7 dB and −26.6 dB. These active element patterns produce a broadside radiation when antenna ports are excited by the following complex weight: $0.25e^{-j0°}$, $0.25e^{-j90°}$, $0.25e^{-j180°}$, and $0.25e^{-j270°}$. The peak radiation gain is observed as 4.6 dBic at $\theta = 0°$, and this is about 6 dB greater than a single antenna in the existence of mutual coupling effects.

III. INTERPRETATION AND ANALYSIS
A. PARAMETRIC STUDY
Fig. 7(a) presents frequency responses of bore-sight gains according to heights of cavity walls. The resonant frequency without the cavity wall is 1.75 GHz with a peak gain of 3.4 dBi and shifts toward the lower frequency points of 1.65 GHz and 1.55 GHz by inserting 3-mm and 6-mm cavity walls, respectively. This implies that the effective dielectric constant can be linearly scaled by the cavity height, which helps to miniaturize the aperture size for individual elements.

To further demonstrate the effectiveness of the proposed design, we employed the same design approach using a conventional probe-fed square patch antenna as
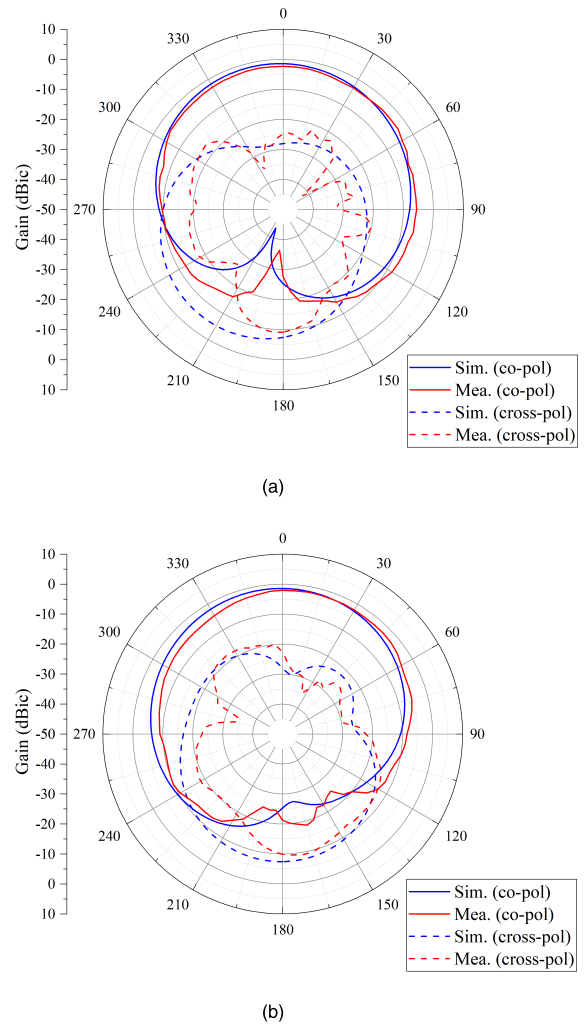

(a)

(b)

FIGURE 6. Measured and simulated radiation patterns. (a) *zx*-plane. (b) *yz*-plane.

shown in Fig. 7(b). For a fair comparison, the antenna characteristics are tuned for the same ceramic substrate ($\varepsilon_r = 20$, $\tan\delta = 0.002$) with dimensions of 21.5 mm × 21.5 mm × 6 mm. The lowest resonant frequency that the antenna could achieve was 1.91 GHz with an edge length of 21 mm and a feeding position of 8 mm from the patch center, as indicated by a blue line. The green line exhibits a frequency response of the conventional antenna when cavity walls surround lateral faces of the substrates. In this structure, a parasitic resonance occurs at around 1.14 GHz unexpectedly due to the cavity dimensions, and the resonance of the square patch remains at the same frequency. These results support that our design approach of scaling the effective dielectric constant can be achieved by accompanying the cavity walls with the proposed coupled feeding structure.

B. EQUIVALENT CIRCUIT MODEL
To interpret operating principles of the proposed structure, we built an equivalent circuit model as illustrated in Fig. 8(a). The feeding pin is modeled as a series inductance, denoted
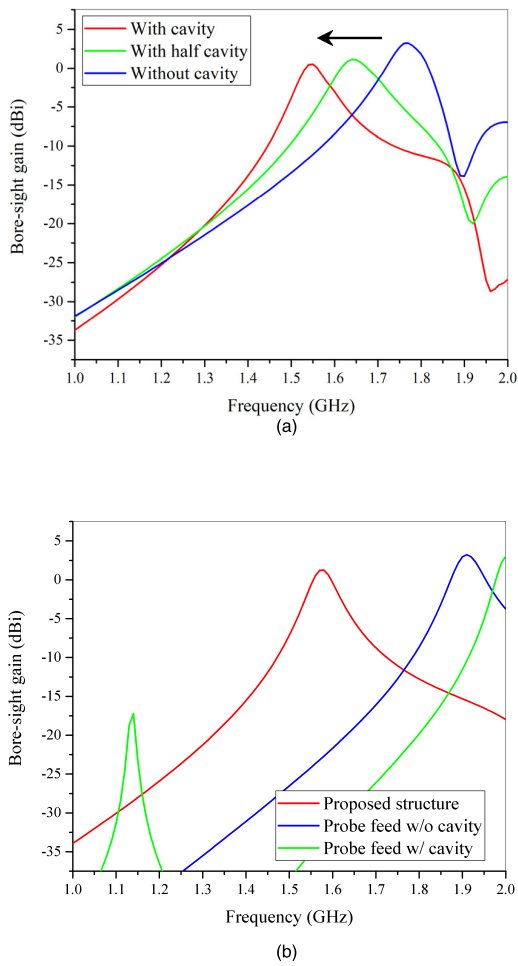
FIGURE 7. Design approach to the proposed structure. (a) Effect of cavity walls. (b) Comparison of feeding structures.

TABLE 2. Values of the equivalent circuit model.

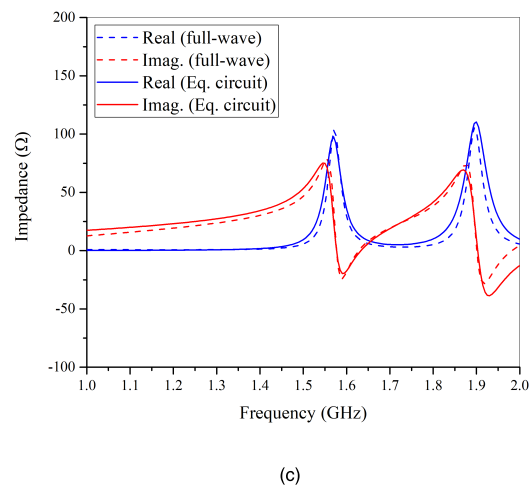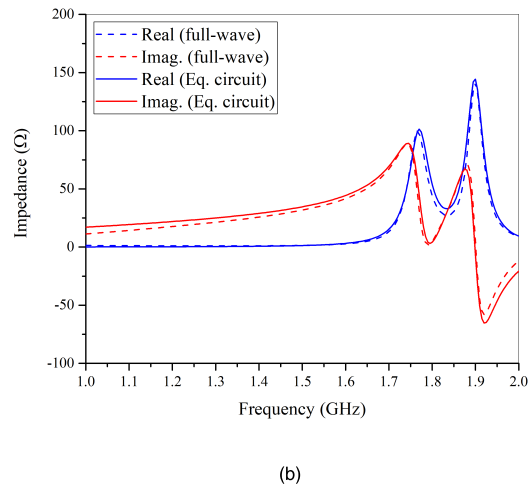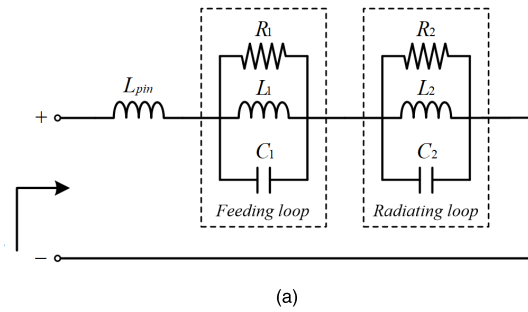| Parameter		Without cavity	With cavity
Feeding pin	L_{pin}	1.895 nH	1.895 nH
Feeding loop	R_I	140	110
	L_I	0.294 nH	0.297 nH
	C_I	23.9 pF	23.9 pF
	$f_{r,feed}$	1915 MHz	1915 MHz
Radiating loop	R_2	97	92
	L_2	0.283 nH	0.283 nH
	C_2	28.57 pF	36.34 pF
	$f_{r,rad}$	1795 MHz	1585 MHz

FIGURE 8. Equivalent circuit model and its impedance responses. (a) Equivalent circuit. (b) Impedance variations without cavity. (c) Impedance variations with cavity.

by L_{pin}, and each loop is expressed as a parallel RLC circuit. Detailed values of the lumped elements are listed in Table 2, and frequency responses of the equivalent circuit model without and with the cavity walls are shown in Figs. 8(b) and 8(c). Note that the resonant frequency of the feeding loop, given as $f_{r,feed}$, remains the same at 1915 MHz although the cavity wall is inserted. On the other hand, the resonance of the radiating loop is shifted from 1795 MHz to 1585 MHz because

C_2 is increased while other values are almost identical. This is due to strong electric fields induced between the outer edge of the radiating loop and the cavity walls at the top layer, which allows to increase ε_{eff} by maximizing the density of near electromagnetic fields within the cavity area.

Fig. 9 provides distributions of magnetic field strengths from the antenna center according to the cavity height. The magnetic fields are calculated in the *zx*-plane
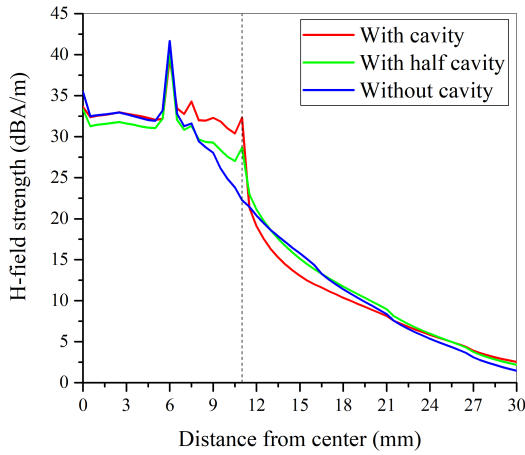
**FIGURE 9.** Variations of H-field strength in proximity to the antenna.

at 61 × 13 points with an interval of 0.5 mm, and magnetic field strengths in the *z*-direction are averaged to calculate each data point. The peak value exists at around 6 mm because of the feeding pin, and the strength tends to decrease as the distance increases. As discussed in the equivalent circuit, the cavity confines near fields within the cavity area; for example, the strengths at 11 mm increase from 22.3 dBA/m to 32.3 dBA/m by inserting the cavity walls.
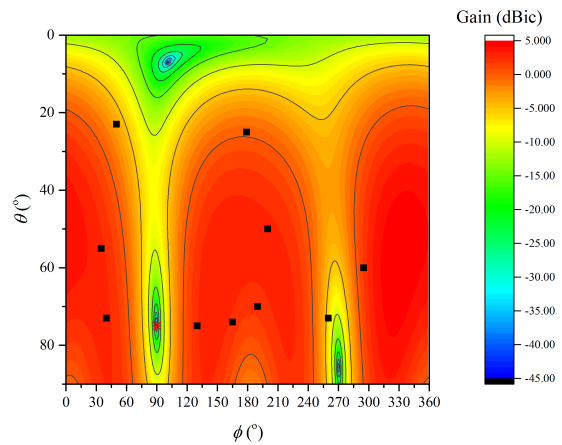
C. ANTI-JAMMING PERFORMANCES
To demonstrate the capability of interference mitigation, the proposed array is applied to an anti-jamming operation based on the power inversion algorithm in (2).

$$\bar{w} = \bar{R}^{-1} \cdot \bar{a}_{jam} \tag{2}$$

This algorithm determines complex weight vector $\bar{w}$ using covariance matrix $\bar{R}$. $\bar{a}_{jam}$ is a steering vector for a jamming direction and is obtained from phase data of measured and simulated active element patterns. Each component of the weighting vector is multiplied to the signal obtained from each array element, and the weighted signals are summed, which corresponds to the signal received by null steering patterns. Fig. 10(a) shows a comparison of null depths according to different jamming powers incident to the array. It is assumed that the noise floor is fixed at about −104.8 dBm, thus, the jamming power of 10^{-5} mW is similar to a jammer-to-noise ratio (JNR) of 50 dB. In our approach, the anti-jamming operation is performed for a single jammer located in the azimuth direction with an angular interval of $\Delta\varphi = 10°$ at $\theta = 75°$. Then, one hundred independent simulations were conducted, and calculated null depths were averaged for more reliable results. Both results tend to decrease as the jamming power becomes weaker, and this tendency agrees well with each other. For instance, null depths obtained using measured and simulated patterns are 44.8 dB and 46.9 dB when the jamming power is 10^{-5} mW. Fig. 10(b) presents an example null-steering pattern calculated using measured active element patterns. The jamming direction is specified by a red '∗'
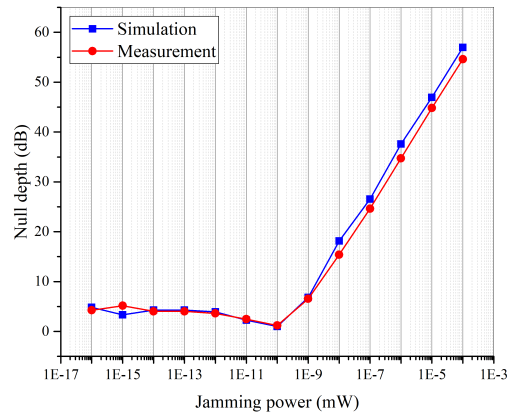
(a)

(b)

FIGURE 10. Anti-jamming performances. (a) Variations of average null depths according to JNR (b) An example null-steering pattern for a jammer located at $\varphi = 90°$ and $\theta = 75°$.

marker, and satellites directions that are taken into account in our simulation are indicated by square markers. As can be seen, the array forms a sharp null with a gain of −36.4 dBic, and gains are maintained to be greater than −5.6 dBic in the satellite directions. The undesired null appears at $\varphi = 270°$ and $\theta = 85°$ because of random noise characteristics, which implies that every snapshot of the null-steering operation produces different array patterns. This irregularity can be resolved by employing an adaptive algorithm, such as the least-mean-square method [26], or using a non-uniform array with more elements. These results confirm that the proposed array can replace the current stand-alone GPS antenna with a capability of interference mitigation.

IV. CONCLUSION
We investigated the design of the coupled-feed structure with cavity walls to miniaturize the antenna aperture by enhancing effective dielectric constants. The measured results showed that the antenna was well-matched with the reflection

coefficient of −14.6 dB, and the mutual coupling was maintained to be less than −9.7 dB ($|S_{21}|$) and −20.7 dB ($|S_{31}|$) for the inter-element spacing of 0.16λ and 0.23λ, respectively. The measured bore-sight gain was −2.51 dBic at 1.575 GHz, and the antenna was circularly polarized with the measured axial ratio of 0.31 dB in the bore-sight direction. It was also verified that the insertion of cavity walls helped to increase the magnetic field strength from 22.3 dBA/m to 32.3 dBA/m in the cavity area, which resulted in the increased effective dielectric constant. The interference mitigation performances were also evaluated based on the power inversion algorithm, and the measured null depth was 44.8 dB for the JNR of 50 dB. The results confirmed that the proposed structure is suitable for use as individual elements of small antenna arrays to replace current single-antenna systems for an additional capability of interference mitigation in an extremely restricted area.

REFERENCES

[1] Q. Liu, Z. N. Chen, Y. Liu, and C. Li, "Compact ultrawideband circularly polarized weakly coupled patch array antenna," *IEEE Trans. Antennas Propag.*, vol. 65, no. 4, pp. 2129–2134, Apr. 2017.

[2] G. Byun, H. Choo, and S. Kim, "Design of a small arc-shaped antenna array with high isolation for applications of controlled reception pattern antennas," *IEEE Trans. Antennas Propag.*, vol. 64, no. 4, pp. 1542–1546, Apr. 2016.

[3] N. Rezazadeh and L. Shafai, "A controlled reception pattern antenna array with dual-mode circular microstrip antenna elements for increased angular availability," *IEEE Trans. Antennas Propag.*, vol. 66, no. 5, pp. 2594–2598, May 2018.

[4] J. A. Maloney, D.-H. Kwon, S. D. Keller, and R. Janaswamy, "Realistic GPS coverage prediction for dual-polarized controlled reception pattern antennas," *IEEE Antennas Wireless Propag. Lett.*, vol. 16, pp. 1907–1910, 2017.

[5] T. Lee, D.-H. Lee, H. Choo, and G. Byun, "A method of substrate shaping to improve gain of active-element pattern for small arrays," *IEEE Antennas Wireless Propag. Lett.*, vol. 16, pp. 1601–1604, 2017.

[6] S. Hwang, B. Lee, D. H. Kim, and J. Y. Park, "Design of S-band phased array antenna with high isolation using broadside coupled split ring resonator," *J. Electromagn. Eng. Sci.*, vol. 18, no. 2, pp. 108–116, Apr. 2018.

[7] G. Byun, H. Choo, and S. Kim, "Improvement of pattern null depth and width using a curved array with two subarrays for CRPA systems," *IEEE Trans. Antennas Propag.*, vol. 63, no. 6, pp. 2824–2827, Jun. 2015.

[8] Z. Qamar, U. Naeem, S. A. Khan, M. Chongcheawchamnan, and M. F. Shafique, "Mutual coupling reduction for high-performance densely packed patch antenna arrays on finite substrate," *IEEE Trans. Antennas Propag.*, vol. 64, no. 5, pp. 1653–1660, May 2016.

[9] S.-Y. Lin and K.-C. Huang, "A compact microstrip antenna for GPS and DCS application," *IEEE Trans. Antennas Propag.*, vol. 53, no. 3, pp. 1227–1229, Mar. 2005.

[10] R. Azadegan and K. Sarabandi, "A novel approach for miniaturization of slot antennas," *IEEE Trans. Antennas Propag.*, vol. 51, no. 3, pp. 421–429, Mar. 2003.

[11] H. Jiang *et al.*, "Miniaturized and reconfigurable CPW square-ring slot antenna loaded with ferroelectric BST thin film varactors," *IEEE Trans. Antennas Propag.*, vol. 60, no. 7, pp. 3111–3119, Jul. 2012.

[12] B. Ghosh, S. K. M. Haque, and N. R. Yenduri, "Miniaturization of slot antennas using wire loading," *IEEE Antennas Wireless Propag. Lett.*, vol. 12, no. 5, pp. 488–491, Apr. 2013.

[13] S. Gupta and G. Mumcu, "Dual-band miniature coupled double loop GPS antenna loaded with lumped capacitors and inductive pins," *IEEE Trans. Antennas Propag.*, vol. 61, no. 6, pp. 2904–2910, Jun. 2013.

[14] X. Xu and J. Wei, "Miniaturisation design of patch antenna using a low-profile mushroom type meta-substrate tailored with high permittivity," *IET Microw., Antennas Propag.*, vol. 12, no. 7, pp. 1216–1221, Jun. 2018.

[15] X. Zhang and L. Zhu, "Gain-enhanced patch antenna without enlarged size via loading of slot and shorting pins," *IEEE Trans. Antennas Propag.*, vol. 65, no. 11, pp. 5702–5709, Nov. 2017.

[16] S. Hwangbo, H. Y. Yang, and Y.-K. Yoon, "Mutual coupling reduction using micromachined complementary meander-line slots for a patch array antenna," *IEEE Antennas Wireless Propag. Lett.*, vol. 16, pp. 1667–1670, Feb. 2017.

[17] M. C. Kang, H. Choo, and G. Byun, "Design of a dual-band microstrip loop antenna with frequency-insensitive reactance variations for an extremely small array," *IEEE Trans. Antennas Propag.*, vol. 65, no. 6, pp. 2865–2873, Jun. 2017.

[18] M. C. Kang, G. Byun, and H. Choo, "Design of a miniaturized dual-band antenna for improved directivity using a dielectric-loaded cavity," *Microw. Opt. Technol. Lett.*, vol. 58, no. 7, pp. 1591–1595, Jul. 2016.

[19] R. T. Compton, "The power-inversion adaptive array: Concept and performance," *IEEE Trans. Aerosp. Electron. Syst.*, vol. 15, no. 6, pp. 803–814, Nov. 1979.

[20] C.-X. Mao, S. Gao, Y. Wang, Q. Luo, and Q.-X. Chu, "A shared-aperture dual-band dual-polarized filtering-antenna-array with improved frequency response," *IEEE Trans. Antennas Propag.*, vol. 64, no. 4, pp. 1836–1844, Apr. 2017.

[21] J. Liu, Z. Tang, Z. Wang, H. Li, and Y. Yin, "Gain enhancement of a broadband symmetrical dual-loop antenna using shorting pins," *IEEE Antennas Wireless Propag. Lett.*, vol. 17, no. 8, pp. 1369–1372, Aug. 2018.

[22] M. K. Mandal and Z. N. Chen, "Compact dual-band and ultrawide-band loop antennas," *IEEE Trans. Antennas Propag.*, vol. 59, no. 8, pp. 2774–2779, Aug. 2011.

[23] M. Ramirez, J. Parron, J. M. Gonzalez-Arbesu, and J. Gemio, "Concentric annular-ring microstrip antenna with circular polarization," *IEEE Antennas Wireless Propag. Lett.*, vol. 10, pp. 517–519, May 2011.

[24] D. M. Pozar, "The active element pattern," *IEEE Trans. Antennas Propag.*, vol. 42, no. 8, pp. 1176–1178, Sep. 1994.

[25] FEKO. (2015). *Altair*. [Online]. Available: http://www.altair.com

[26] O. L. Frost, III, "An algorithm for linearly constrained adaptive array processing," *Proc. IEEE*, vol. 60, no. 8, pp. 926–935, Aug. 1972.

GANGIL BYUN (S'12–M'15) received the B.S. and M.S. degrees in electronic and electrical engineering from Hongik University, Seoul, South Korea, in 2010 and 2012, respectively, and the Ph.D. degree in electronics and computer engineering from Hanyang University, Seoul, in 2015. After his graduation, he returned to Hongik University to work as a Research Professor and performed active research for two years. He joined the Faculty of Ulsan National Institute of Science and Technology, in 2018, where he is currently an Assistant Professor of electrical and computer engineering.

His research interests include the design and analysis of small antenna arrays for adaptive beamforming applications, such as the direction of arrival estimation, interference mitigation, radar, circularly-polarized antennas, vehicular and aeronautic antennas, global positioning system antennas, and antenna and array configuration optimization. He has actively contributed to the consideration of both antenna characteristics and signal processing perspectives for the improvement of overall beamforming performances.

JUN HUR (S'16) received the B.S. and M.S. degrees in electronic and electrical engineering from Hongik University, Seoul, South Korea, in 2014 and 2016, respectively, where he is currently pursuing the Ph.D. degree in electronics and computer engineering.

His research interests include the global positioning system antennas, antenna arrays, and position optimization of array elements for adaptive beamforming.

SEUNG-SEOK KANG received the B.S. and M.S. degrees in electronic and electrical engineering from Hongik University, Seoul, South Korea, in 2015 and 2018, respectively. He joined as an Assistant Research Engineer of Navcours Co, Ltd., in 2018.

His current research interests include the design and analysis of small antenna arrays for anti-jamming systems.

SEOK BO SON received the B.S., M.S., and Ph.D. degrees in electronics engineering from Chungnam National University, in 1996, 1998, and 2002, respectively. He has been an Adjunct Professor of electronics engineering with Chungbuk National University, since 2006. He is with Navcours Co., Ltd., where he is currently the Director. His current research interests include alternative navigation system, high quality antenna, and smart jamming system design.

HOSUNG CHOO (S'00–M'03) received the B.S. degree in radio science and engineering from Hanyang University, Seoul, in 1998, and the M.S. and Ph.D. degrees in electrical and computer engineering from The University of Texas at Austin, in 2000 and 2003, respectively. In 2003, he joined the School of Electronic and Electrical Engineering, Hongik University, Seoul, South Korea, where he is currently a Full Professor.

His current research interests include the use of the optimization algorithm in developing antennas and microwave absorbers. His studies include the design of small antennas for wireless communications, reader and tag antennas for RFID, and on-glass and conformal antennas for vehicles and aircraft.

● ● ●